

Adsorption of soluble oil from water to graphene

Na Wang · Yuchang Zhang · Fuzhen Zhu · Jingyi Li ·
Shuaishuai Liu · Ping Na

Received: 6 September 2013 / Accepted: 22 December 2013 / Published online: 14 February 2014
© Springer-Verlag Berlin Heidelberg 2014

Abstract The toxicity of soluble oil to the aquatic environment has started to attract wide attention in recent years. In the present work, we prepare graphene according to oxidation and thermal reduction methods for the removal of soluble oil from the solution. Characterization of the as-prepared graphene are performed by scanning electron microscopy, transmission electron microscopy, X-ray diffraction, Raman spectra, Brunauer-Emmett-Teller, X-ray photoelectron spectroscopy, and contact angle analysis. The adsorption behavior of soluble oil on graphene is examined, and the obtained adsorption data are modeled using conventional theoretical models. Adsorption experiments reveal that the adsorption rate of soluble oil on graphene is notably fast, especially for the soluble diesel oil, which could reach equilibrium within 30 min, and the kinetics of adsorption is perfectly consistent with a pseudo-second-order model. Furthermore, it is determined that the adsorption isotherm of soluble diesel oil with graphene fit the Freundlich model best, and graphene has a very strong adsorption capacity for soluble diesel oil in the solution. These results demonstrate that graphene is the material that provided both good adsorptive capacity and good kinetics, implying that it could be used as a promising sorbent for soluble oil removal from wastewater.

Keywords Graphene · Oil spill · Soluble oil · Toxicity · Contact angle · Adsorption capacities

Responsible editor: Angeles Blanco

N. Wang · Y. Zhang · S. Liu · P. Na (✉)
School of Chemical Engineering and Technology, Tianjin University,
Tianjin 300072, People's Republic of China
e-mail: naping@tju.edu.cn

F. Zhu · J. Li
TEDA Lando Oilfield Service Co., Ltd., Tianjin 300457, People's
Republic of China

Introduction

Following an accidental oil spill at sea, the collection and removal of surface oil over a large area are usually the primary concern for decreasing energy loss and damage to the environment. However, the treatment of dissolved oil retained in deep-water columns should not be ignored, as the dissolved oil is the most available to marine biota (Kennedy and Farrell 2005, Neff and Anderson 1981). The early impact of the spilled product on marine life will rely on the composition and concentration of the soluble fraction. From this point of view, aromatic hydrocarbons are of special concern as they exhibit higher solubility and toxicity in the aquatic environment (Gonzalez et al. 2006). Greater acute toxicity is generally associated with the lower molecular weight polycyclic aromatic hydrocarbons (PAHs) (Gonzalez et al. 2006, Le Dû-Lacoste et al. 2013, Meador et al. 1995). In fact, many of these compounds appear in the priority pollutant list of the United States Environmental Protection Agency (USEPA) (Hannam et al. 2010, Harper et al. 1996). Even though the potential effects of dissolved oil on marine life has been paid much attention, only a small number of studies to date have proposed effective methods for managing the water-soluble fraction (WSF) of oil spills. To the best of our knowledge, the main techniques that are useful for cleaning up the soluble oil are biological treatment (Atlas 1981) and photocatalytic destruction (Zioli and Jardim 2002a), but removing the soluble oil from the deep-water column always takes a long time when these methods are used. In addition, even though many researchers have extensively investigated natural materials (Korhonen et al. 2011, Radetic et al. 2008, Wang et al. 2012), synthetic materials (Hayase et al. 2013, Nicolas et al. 2006), and graphite-based materials (Cong et al. 2012, Sun et al. 2013, Toyoda and Inagaki 2003) as potential sorbents for the removal of floating oil in large area from water, research on the soluble oil sorption capability of these sorbents, particularly graphene, has not been reported.

Graphene, a two-dimensional structure of carbon hexagons consisting of sp^2 -hybridized C–C bonds with a π -electron cloud (Allen et al. 2010, Stankovich et al. 2006), has attracted a great deal of scientific interest in recent years. Due to its extremely high surface area (Stankovich et al. 2006) and hydrophobic nature (Wang et al. 2009), it can be used as an adsorbent. The focus on the removal of toxic compounds from contaminated water by graphene is emerging. Iqbal and Abdala (2012) demonstrated that graphene has excellent sorption capacity for the removal of floating oil, with sorption capacity as high as 131 g g^{-1} . Ji et al. (2013) also investigated the removal of naphthalene, 2-naphthol, and 1-naphthylamine in wastewater by graphene via π - π electron donor–acceptor interactions. The adsorption of pyridine and its derivatives on the graphene surface has been studied using density functional theory (DFT) (Voloshina et al. 2011). From earlier-reported literatures, it is known that the aromatic compound can easily adsorb on graphene by π - π stacking. Therefore, graphene could be an excellent candidate for the removal of dissolved oil with a low concentration, which mainly consists of lower molecular weight polycyclic aromatic hydrocarbons. Currently, three graphene preparation methods have been reported, including the micromechanical exfoliation of graphite (Meyer et al. 2007, Novoselov et al. 2004), the reduction of graphite oxide (McAllister et al. 2007, Schniepp et al. 2006, Stankovich et al. 2007), and chemical vapor deposition (CVD) (Kim et al. 2009, Ueta et al. 2004). Among these methods, graphene prepared by the thermal exfoliation of graphite oxide seems to be best because this graphene possesses a high surface area and a smaller number of layers (Steurer et al. 2009). Moreover, the thermal exfoliation of graphite oxide technique is relatively easy, and hazardous reductants are not used. Furthermore, the most exciting advantages of this method are its low-cost and massive scalability.

In this work, we prepare graphene by the oxidation and thermal reduction methods. Moreover, the as-prepared graphene is characterized by scanning electron microscopy (SEM), transmission electron microscopy (TEM), X-ray diffraction (XRD), Raman spectra, Brunauer-Emmett-Teller (BET), X-ray photoelectron spectroscopy (XPS), and contact angle analysis. Additionally, to achieve a comprehensive understanding of the adsorption capacity of graphene on soluble oil, we test two typical dissolved oils—diesel oil and crude oil—to investigate the adsorption performance of graphene on each soluble oil. More importantly, we also quantify the soluble oil sorption (milligrams per gram) of graphene and discuss its adsorption mechanism.

Experimental

Materials

Graphite flakes (~50 mesh, 99.995 %) and expandable graphite were obtained from Qingdao Haida Graphite Co., Ltd.

Activated carbon with a particle size range between 0.5 and 2.0 mm was provided by Cuihong Technology Co., Ltd. Sulfuric acid (98 %), sodium nitrate, potassium permanganate, hydrogen peroxide (30 %), hydrochloric acid (37 %), barium chloride, silver nitrate, and *n*-hexane were purchased from Tianjin Jiangtian Chemical Reagents Co., Ltd., China. Diesel oil was collected from a local service station and crude oil was provided by CNOOC Ltd. Tianjin Company. The experimental oil properties are listed in Table 1.

Preparation of graphite oxide

Graphite oxide was prepared according to the Hummers–Offeman method (Steurer et al. 2009), whose principal steps include the oxidation of graphite in concentrated H_2SO_4 with NaNO_3 and KMnO_4 . In brief, 10 g of the graphite powder were added into a 1,000-mL beaker, and 5 g of NaNO_3 and 250 mL of H_2SO_4 were subsequently added while stirring. After 1 h of stirring, the dispersion was cooled to 8°C using an ice-water bath. Next, 30 g of KMnO_4 were added slowly into the beaker over the course of 5 h under stirring conditions, and the temperature of the dispersion was controlled up to 20°C . Later, the ice-water bath was removed and the mixture was stirred at room temperature for 2 h. Next, the reaction was quenched by pouring the dispersion into 500 ml of ice water. Next, an aqueous solution of H_2O_2 was added to reduce the residual KMnO_4 until the bubbling ceased. Finally, the produced graphite oxide was washed with aqueous HCl until no sulfite ions were detected and then washed with water until no chloride ions were detected. The brown graphite oxide was dried by vacuum at 60°C for 12 h.

Thermal reduction of the graphite oxide and preparation of expanded graphite

Thermal exfoliation of graphite oxide was performed by placing the dry graphite oxide (0.5 g) into a crucible that was sealed at the end. Then, the crucible was placed in a muffle furnace and was rapidly heated to approximately $1,000^\circ\text{C}$ for 30 s under a nitrogen atmosphere (Iqbal and Abdala 2012). The resulting graphene was a black powder with very low bulk density (5.7 g L^{-1}). Expanded graphite was prepared by placing expandable graphite in a muffle furnace at approximately 1000°C for 30 s.

Table 1 Properties of the experimental oils at room temperature

Oil type	Density (g/cm^3)	Viscosity (cP)	Surface tension (MN/m)
Diesel oil	0.839	6.5	12.8
Crude oil	0.859	79.8	15.4

Obtaining the WSF

For each tested oil sample, a flask filled with 5 L water was used. Twenty-five milliliters (25 ml) of oil was added, and the solution was mechanically stirred for 12 h. For experiments in the absence of light, the flask was allowed to equilibrate undisturbed for up to 45 days in the dark at room temperature. Then, the mixture located 5 cm under the surface was slowly transferred to another container by an oil-repellent glass bend pipe, and the obtained mixture was exactly the WSF that we needed (Zioli and Jardim 2002b).

Sorption capacities of synthesized graphene

The adsorption experiments for the two tested oil samples were performed in a similar manner. All the absorption tests were performed at 25±3 °C. The simulated soluble oil (50 ml) was acidized with 0.5 ml sulfuric acid (1:3, v/v) and later extracted by 10 mL *n*-hexane using a 125-mL separating funnel two times; subsequently, the above liquid was transferred to a 25-ml volumetric flask, and the volume was completed to 25 ml with *n*-hexane. The concentration of the resulting solution was measured by an ultraviolet spectrophotometer using a calibration curve prepared by measuring various known concentrations of the soluble oil solutions. The concentration of the simulated soluble oil (C_{oil}) was calculated using the following equation:

$$C_{oil} = Q \left(\frac{V_1}{V_2} \right)$$

where Q (milligrams per liter) is the concentration of the extracted liquid, V_1 (milliliters) is the volume of the extracted liquid, and V_2 (milliliters) is the volume of the simulated soluble oil solution.

For the adsorption kinetic study, 0.01 g of graphene was added to 50 ml of the simulated oil sample, and the mixture was stirred in a water bath. After a specified time, the solid and liquid phases were separated by separating funnel immediately and analyzed to measure the concentration of the dissolved oil in the remaining solution, using the method mentioned above. For the adsorption isothermal study, the simulated soluble oil was diluted to prepare a series of solutions with different

concentrations. Then, 0.01 g of the adsorbent was added to 50 mL of the solutions with different concentrations while stirring in a water bath for 4 h. In order to compare with other adsorbents, 0.01 g of graphene, 0.01 g of expanded graphite, and 0.1 g of active carbon was added to 50 ml of soluble diesel oil, respectively. Then, the mixtures were stirred in a water bath for a long time to reach balance. The adsorption capacity (q_{oil}) for the dissolved oil was obtained from the following equation:

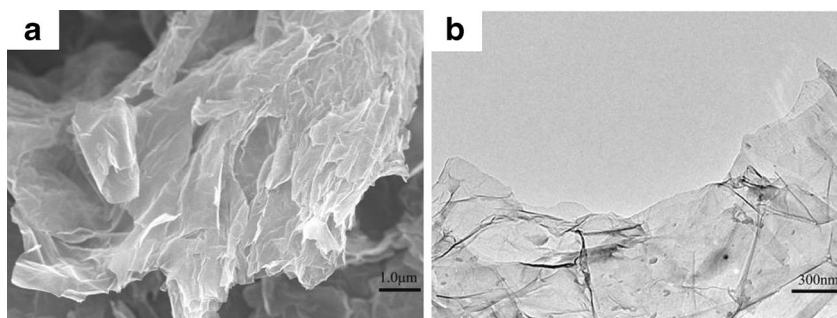
$$q_{oil} = \frac{(C_0 - C_R)V}{W}$$

where V (milliliters) is the volume of simulated oil solution, C_0 and C_R (moles per liter) are the concentrations of initial and remaining dissolved oil respectively, and W (grams) is the weight of graphene.

Characterization of graphene

XRD analysis was performed on a Bruker AXS D8 Focus X-ray diffractometer (Germany) equipped with Cu K α radiation ($\lambda=0.1542$ nm). The patterns were recorded from 10 to 35° with a step size of 0.02°/s at 40 kV voltage with an intensity of 40 mA. Raman spectra were obtained on a laser Raman spectrometer (DXR Microscope, American) with an excitation wavelength of 532 nm at room temperature. N₂ adsorption-desorption isotherms were measured at 77 K using a NOVA-2000 volumetric gas sorption instrument (Quantachrome, USA). The total surface area was calculated by the BET method, while the pore size distribution was obtained from the Barrett-Joyner-Halenda (BJH) equation. Prior to the measurement, the sample was degassed overnight at 200 °C. TEM was performed with a JEM-2100F (JEOL, Japan) at an accelerating voltage of 100 kV. SEM image was obtained with a Hitachi S4800 SEM (Hitachi, Japan). The XPS of the samples was observed on a Perkin-Elmer PHI 1600 ESCA X-ray photoelectron spectroscope with a monochromatic Mg K α radiation (1,253.6 eV) and the binding energies were normalized to C1s peak at 284.6 eV. The static and dynamic contact angle between the graphene and the experimental oils were measured using an optical contact angle measuring device (Dataphysics OCA-20, Germany)

Fig. 1 SEM image (a) and TEM image (b) of graphene



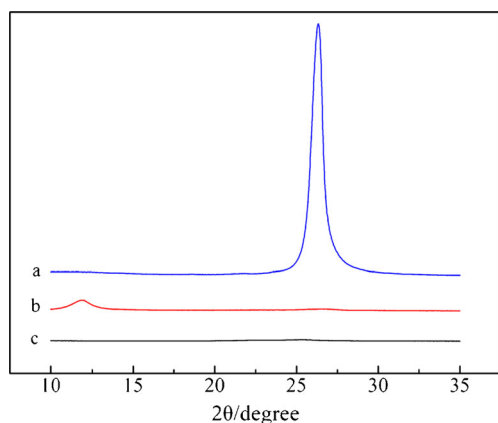


Fig. 2 XRD patterns of graphite (a), graphite oxide (b) and graphene (c)

equipped with a charge-coupled device (CCD) camera to capture images and video of the solid/liquid interface.

Results and discussion

Characterization of graphene

The morphology and nanostructure of graphene were characterized by SEM and TEM observations. Figure 1a showed the SEM image of the graphene, and it was clear that the curled and wrinkled graphene sheets stacked together in a disordered fashion to form a porous structure. Transparent sheets with a large number of dark ripples were observed in the TEM image, which was presented in Fig. 1b. The transparency revealed that graphite oxide had been successfully exfoliated (Iqbal and Abdala 2012, Pan et al. 2009).

X-ray diffraction was used to determine any changes to the interlayer distance between the nanosheets, which was an important parameter to evaluate for obtaining structural

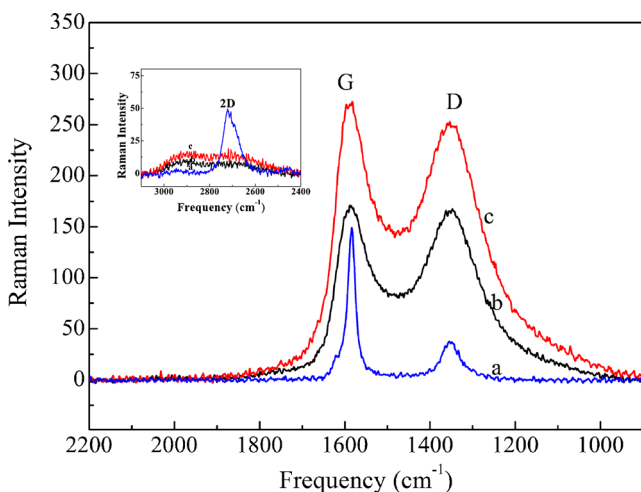


Fig. 3 Evolution of the Raman spectra during the oxidation and exfoliation processes for graphite (a), graphite oxide (b) and graphene (c)

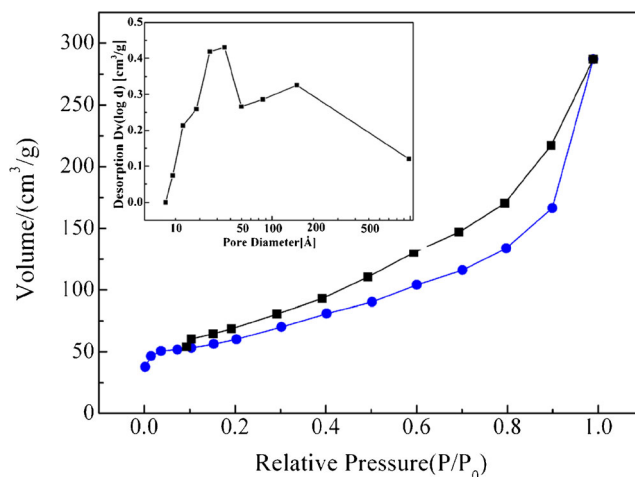
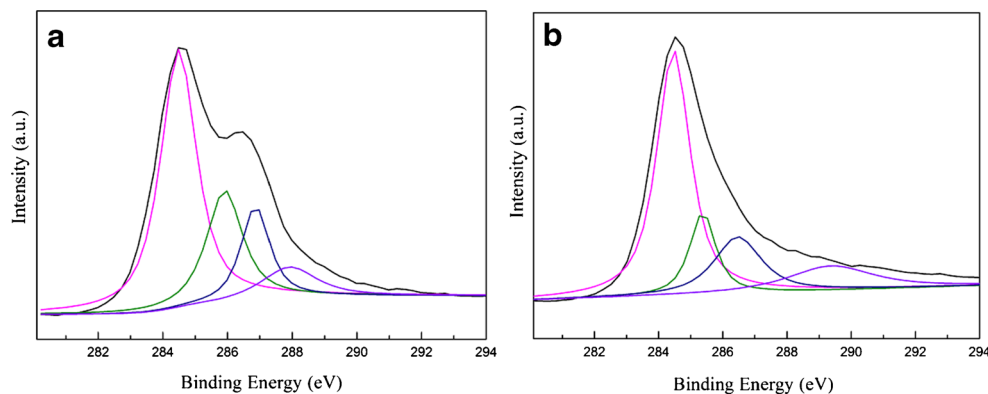


Fig. 4 Nitrogen adsorption-desorption isotherm and pore size distributions for graphene

information on the graphene. Figure 2 showed the XRD patterns of graphite, graphite oxide and graphene. As oxidation proceeded, the intensity of the (002) diffraction peak, which was an intrinsic peak of graphite exhibiting the stacked graphene layers, appeared at $2\theta=26.35^\circ$, corresponding to a d-spacing of 0.338 nm, and gradually weakened and finally disappeared. Simultaneously, a peak at $2\theta=11.8^\circ$ appeared, which corresponded to the (001) diffraction peak of graphite oxide, indicating interlayer expansion to a d-spacing of 0.75 nm and was due to the presence of oxide functionalities and the adsorbed water intercalation (Lerf et al. 2006, Zhao et al. 2010). These results suggest that the layer-to-layer distance was enlarged and the graphite had been completely oxidized. After thermal reduction, the diffraction line showed a typical broad trace with an obvious disappearance of the characteristic peaks, implying that the graphite oxide had successfully exfoliated to form a monolayer or a few layers (Chen et al. 2010, Wang et al. 2009, Zhao et al. 2010).

Significant structural changes during the chemical processing from graphite to graphite oxide and to graphene sheets could also be characterized by Raman spectroscopy, as shown in Fig. 3. The spectrum revealed some useful information, for example, structural disorder (D band), the relative motion of the sp^2 carbon atoms (G band) and the stacking order (2D band) (Ferrari et al. 2006, Ferrari and Robertson 2000, Kudin et al. 2008). On the one hand, the integrated intensity ratio of the D and G bands (I_D/I_G) was a measure of the disorder degree and average size of the sp^2 domains (Ferrari and Robertson 2000, Pan et al. 2009). Comparing the spectrum of the graphite with that of graphite oxide, we could see that the I_D/I_G increased dramatically, and the G band became broader and more symmetric. Moreover, the G band initially shifted to higher frequencies (from $\sim 1,583$ to $\sim 1,587$ cm^{-1}). These results implied that the carbon-carbon double bond in the graphene lattice was destroyed, resulting in an increase in a considerable amount of structural disorder by the oxidation

Fig. 5 XPS C 1s spectra of graphite oxide (a) and graphene (b)



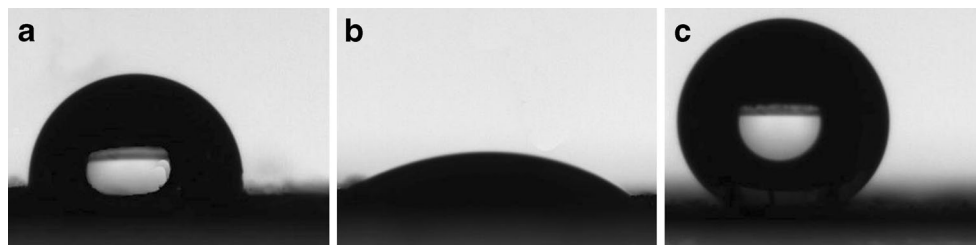
process (Meador et al. 1995, Pan et al. 2009, Paredes et al. 2009). When a Raman spectrum of graphene was compared with that of graphite oxide, the I_D/I_G ratio decreased slightly, suggesting that the aromaticity of the graphene lattice was restored after the thermal reduction. Moreover, the G band of the graphene was somewhat sharpening and shifted back in position ($\sim 1,584\text{ cm}^{-1}$), which attributed to a graphitic “self-healing” (Han et al. 2001, Kudin et al. 2008, Sato et al. 2006). Nevertheless, comparing the spectrum of graphene with that of graphite, the intensity of the D band increased substantially, which demonstrated that during the oxidation and thermal exfoliation process, the carbon lattice possesses highly defected areas but returns to an essentially graphitic state. On the other hand, the shape of the 2D peak was used to distinguish between single-layer graphene, bilayer graphene, and the bulk graphite. Bilayer sheets or sheets with less than five layers have a broader and symmetrical 2D peak, while bulk graphite exhibited a distorted peak (Iqbal and Abdala 2012). The Raman spectrum of graphene showed a broader and symmetrical 2D peak in the $2,600$ to $2,900\text{ cm}^{-1}$ range, indicating that the graphene sheets with less than five layers were obtained after thermal exfoliation.

The N_2 adsorption-desorption isotherm and pore size distribution of the graphene were shown in Fig. 4. The isotherm exhibited a standard Langmuir-type curve at low relative pressure, pertaining mainly to surface coverage and the filling of the sample pores. At the same time, a hysteresis loop was clearly visible at high relative pressure, suggesting the formation of a mesopore, which also had been confirmed by the SEM results. The pore size distribution curves calculated by the BJH method further confirmed that the majority of the

graphene nanosheet pores had a pore width between 2 and 25 nm (within the mesopore range). Moreover, its bimodal pore size distribution provided oil soluble molecules suitable access to the interior (Leinweber et al. 2002). The graphene nanosheets had a surface area of $290\text{ m}^2\text{ g}^{-1}$, which was substantially smaller than the theoretical surface area of $2,620\text{ m}^2\text{ g}^{-1}$ for single-layer graphene sheets (Stankovich et al. 2006) and partially due to overlap and the stacking of exfoliated layers.

XPS analysis has been performed on both graphite oxide and graphene samples and the high resolution C1s spectrum is plotted in Fig. 5. The C1s XPS spectrum of GO (Fig. 5a) clearly showed four main peaks at 285, 286.7, 287.3, and 288.9 eV corresponding to C=C, C-O, C=O, and O=C-OH functional groups, respectively, indicating the presence of a large fraction of hydrophilic moiety in GO (Dreyer et al. 2010, Yang et al. 2009). However, the two peaks (C=O, O=C-OH) at 287.3 and 288.9 eV almost disappeared and the peak (C-O) at 286.7 eV slightly decreased after thermal treatment, as shown in Fig. 5b. This also confirms that the thermal reduction of GO significantly reduced the oxygen content in the samples, changing the surface from hydrophilic into hydrophobic. To further confirm their hydrophobic characteristics, water contact angle measurement was also used and the results were shown in Fig. 6a–c. It was observed that the contact angle decreased from 95.9° to 29.4° after the graphite oxidation process, whereas then increased from 29.4 to 149.8° after the thermal reduction of graphite oxide, which consistent with the XPS results. And it was interesting to note that the contact angle of graphene was larger than that of graphite. This result was quite unexpected and apparently contradicted the idea

Fig. 6 Optical image of a water droplet on a graphite film at a CA of 95.9° (a), a graphite oxide film at a CA of 29.4° (b) and a graphene film at a CA of 149.8° (c)



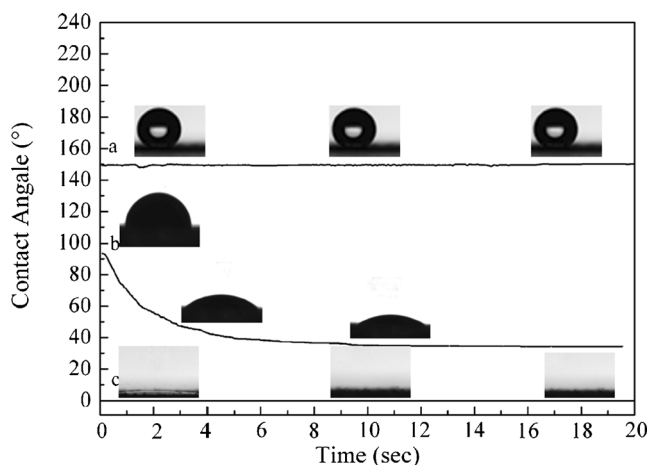


Fig. 7 Dynamic contact angle measurement of a water droplet (a), crude oil droplet (b) and diesel oil droplet (c) onto graphene film: contact angle variation with time

that the partial hydroxyl and carboxyl group could not be reduced, which resulted in the hydrophobic characteristics of graphite being stronger than those of graphene. However, water repellency which was an interfacial behavior also depended on the surface roughness on a multiple scale (Hsieh and Chen 2010), such as lotus leaf. As observed in Fig. 1b, the graphene powders offered a primary roughness whereas the flake-like voids between the nanosheets generated a secondary roughness which allowed an air pocket into the roughened structure, and then the existing air film in the roughened structure was capable of providing a floating force to resist water penetration, thus inducing the contact angle of graphene was larger than that of graphite (Hsieh and Chen 2011). Previous work also reported that graphene showed a low surface energy and large contact angle in comparison with graphite (Wang et al. 2009).

Furthermore, the variation of the dynamic contact angles with time of the two types of experimental oils on the graphene film were also performed, which was described in Fig. 7. The results indicated that water formed a stable droplet on the surface of the graphene film and generally did not spread over time. Meanwhile, the diesel oil droplet had completely spread immediately upon contacting the graphene

Fig. 8 Soluble diesel oil (a) with the initial concentration of 76.86 mg L^{-1} and crude oil (b) with the initial concentration of 2.638 mg L^{-1} adsorption kinetics onto graphene

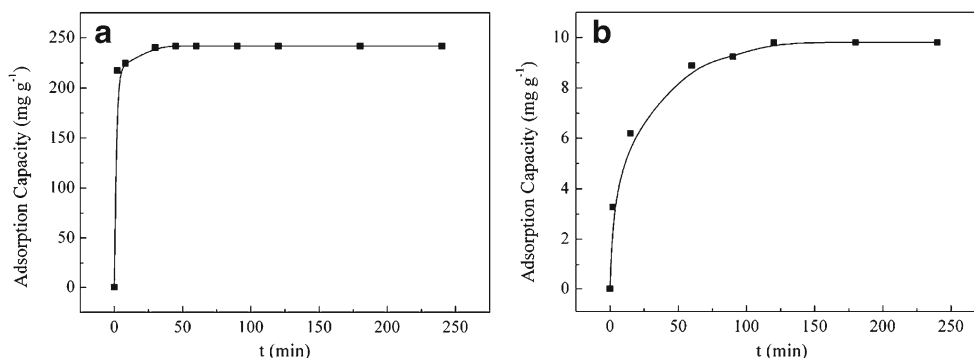


Table 2 Comparison of equilibrium sorption capacity of soluble diesel oil on various adsorbents

Adsorbent	Equilibrium sorption capacity (mg g^{-1})	Reference
Graphene	241.88	This work
Expanded graphite	178.64	This work
Activated carbon	113.97	This work
Cellulose fiber	60	Li et al. (2012)

film. In the case of crude oil droplets, the contact angle became 34.3° after 20 s. This result indicated that graphene was a superoleophilic-superhydrophobic material.

Adsorption kinetics

The ability of graphene to act as an adsorbent for soluble oil removal was tested. Figure 8 showed the adsorption kinetics curve of soluble diesel oil and soluble crude oil to analyze the adsorption behavior of trace oil on graphene. The results showed that the soluble diesel oil adsorption rate occurred more quickly, achieving balance within 30 min (Fig. 8a), and the soluble crude oil adsorption rate was very fast during the first 40 min, and the equilibrium was established after 2 h (Fig. 8b). The process of adsorption achieved equilibrium in such a short time, suggesting that graphene had a very high adsorption efficiency and, therefore, high-value industrial applications. Lower values of surface tension and viscosity suggested that the soluble oil penetrated the graphene pore structure and was adsorbed on the solid sorbent more easily. These results were consistent with our previously reported work (Li et al. 2012). Additionally, the achieved equilibrium sorption capacity was more than 500 times lower than the maximum reported capacity for graphene for sorption of crude oil from the water surface (Iqbal and Abdala 2012), which could be mainly attributed to that the initial concentration of soluble crude oil is very low (2.638 mg L^{-1}) in this study while the large mass of crude oil was onto the water surface (10 mL crude oil per 50 mL water) in that report (Iqbal and

Abdala, 2012). Kannan and Sundaram (2001) demonstrated that the amount adsorbed increased exponentially with the increase in initial concentration of adsorbate. Similar results have been reported in literature on the extent of removal of dyes [Deo and Ali 1993, Mckay et al. 1985] and metal ions [Kannan 1991]. In order to compare the adsorption effect of other adsorbents on soluble oil, expanded graphite and activated carbon were also studied and the relevant equilibrium sorption capacities are given in Table 2. It showed that the graphene studied in this work has very large adsorption capacity.

To investigate the adsorption properties further, the pseudo-first-order (Langergren and Svenska 1898) and pseudo-second-order (Ho and McKay 1998) kinetics and the intraparticle diffusion model (Weber and Morris 1963) were selected to simulate the adsorption kinetics curve. The rate equations were described as Eqs. 1a, 1b and 1c, respectively.

$$-\ln(q_e - q_t) = k_1 t - \ln q_e \tag{1a}$$

$$\frac{t}{q_t} = \frac{1}{k_2 q_e^2} + \frac{1}{q_e} \tag{1b}$$

$$q_t = k_p t^{1/2} + c \tag{1c}$$

where k_1 (grams per milligram per minute), k_2 (grams per milligram per minute) and k_p (grams per milligram per square root minute) are the rate constants of the first-order kinetic

model, second-order kinetic model, and intraparticle diffusion model, respectively; q_t (milligrams per gram) and q_e (milligrams per gram) are the adsorption capacity of soluble oil at time t (minutes) and at the equilibrium state, respectively. C is the constant.

The results of fitting these models were shown in Fig. 9, and the fitting parameters, linear regression coefficient (R^2) and standard deviation (SD) of all the kinetic models were calculated and listed in Table 3. Generally, the higher was the value of R^2 and the lower was the value of standard deviation (SD), the better would be the goodness of fit. As seen in Table 3, the pseudo-first-order kinetic model ($R^2 < 0.9652$) for soluble oil adsorption fit worse in comparison with the pseudo-second-order model ($R^2 > 0.995$, $SD < 0.1197$). In addition, the calculated q_e values from the pseudo-second-order model were much closer to the experimental values, $q_e(\text{exp})$. This finding suggested that the adsorption of soluble oil on graphene could be described using a pseudo-second-order kinetic model.

Due to the porous structure of the graphene, the diffusion of the soluble oil from the external surface to the pores via boundary layer diffusion and within the pores of the adsorbent could not be ignored. In this study, the intraparticle diffusion model was applied to identify the diffusion mechanism of the soluble oil adsorption onto the graphene. Figure 9c, f showed that the adsorption plots were not linear over the whole time range and could be separated into a few linear regions. This represented that there were two stages taking place. The one stage was external surface adsorption that the adsorbate

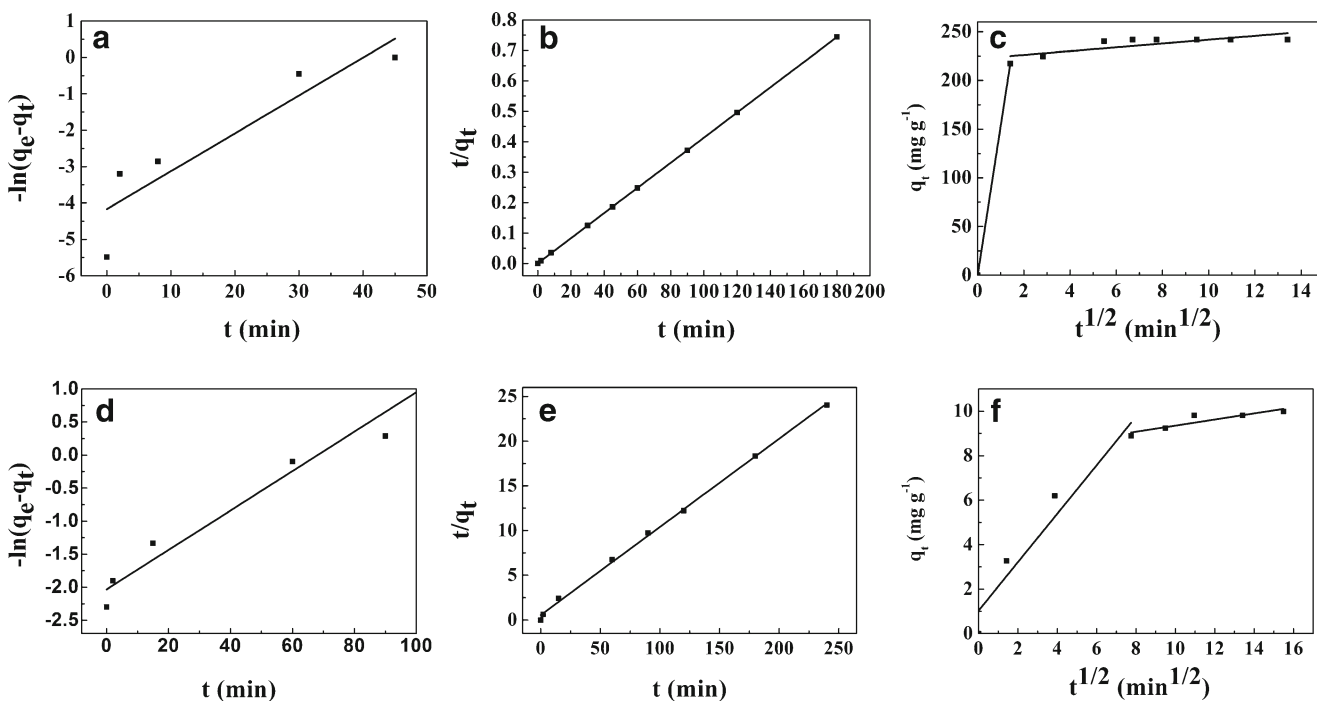


Fig. 9 Pseudo-first-order kinetic plots for the adsorption of soluble diesel oil (a) and soluble crude oil (d), pseudo-second-order kinetic plots for the adsorption of soluble diesel oil (b) and soluble crude oil (e), intraparticle diffusion model for the adsorption of soluble diesel oil (c) and soluble crude oil (f)

Table 3 Kinetic parameters for the adsorption of experiment oil by graphene

Sample	Pseudo-first-order model			Pseudo-second-order model			Intraparticle diffusion model										
	C_0 (mg l ⁻¹)	q_e (exp) (mg g ⁻¹)	q_e (cal) (mg g ⁻¹)	K_1 (min ⁻¹)	R^2	SD	q_e (cal) (mg g ⁻¹)	K_2 (g mg ⁻¹ min ⁻¹)	R^2	SD	K_{p1} (g mg ⁻¹ min ^{-1/2})	R^2	SD	K_{p2} (g mg ⁻¹ min ^{-1/2})	C	R^2	SD
Diesel oil	76.86	241.8	64.59	0.1041	0.9468	0.08102	243.9	0.001870	0.9999	6.499×10 ⁻⁷	–	–	–	1.953	222.3	0.5926	38.91
Crude oil	2.638	9.980	7.230	0.03040	0.9652	0.08025	10.02	0.01966	0.9984	0.1197	1.089	0.9049	1.387	0.1374	7.973	0.7741	0.04882

diffused through the solution to the external surface of the adsorbent or the boundary layer diffusion of solute molecules, where the adsorption rate was high. The second stage was that soluble molecules were entered into the graphene particles by intraparticle diffusion through pores (Vimonses et al. 2009). It was clear that both straight lines did not pass through the origin, suggesting that the intraparticle diffusion was not the sole rate-limiting step (Ho et al. 2000). The calculated values of k_{d2} increased with the increase of the adsorbent dose and the initial concentration of soluble oil. This could be due to the concentration gradient existing between the bulk solution and the surface of the substrate, acting as a driving force for mass transfer (Maatar et al. 2013). As seen in Table 3, the k_{d2} value of soluble diesel oil was large in comparison with crude oil, since its initial concentration was larger than crude oil. Furthermore, the value of the intercept C gave an idea about the film transfer caused by the diffusion of the adsorbate from the bulk solution to the adsorbent surface. The larger the intercept was, the greater was the boundary layer effect (McKay et al., 1985). The boundary layer effect on diffusion process of soluble diesel oil was greater than crude oil. So the boundary layer diffusion was the rate-limiting step. Previous reports also demonstrated that the boundary layer diffusion was the rate controlling step in systems characterized by low concentrations of adsorbate, poor mixing, and small particle size of adsorbent (Ray 1996, Mohan and Singh 2004).

Adsorption isotherms

To thoroughly understand the adsorption process, we obtained adsorption isotherms of soluble diesel oil with different initial concentrations ranging from 8 to 70 mg L⁻¹, as shown in Fig. 10a. The curves showed that the adsorption capacities increased with the increase in adsorbate equilibrium concentration, and the slopes of the adsorption isotherms decreased gradually. Three classic adsorption models, including the Langmuir, Freundlich, and Temkin models, were used to describe the adsorption equilibrium. The mathematical representations of the Langmuir (1916), Freundlich (1906), and Temkin (Temkin and Pyzhev 1940) models were given below:

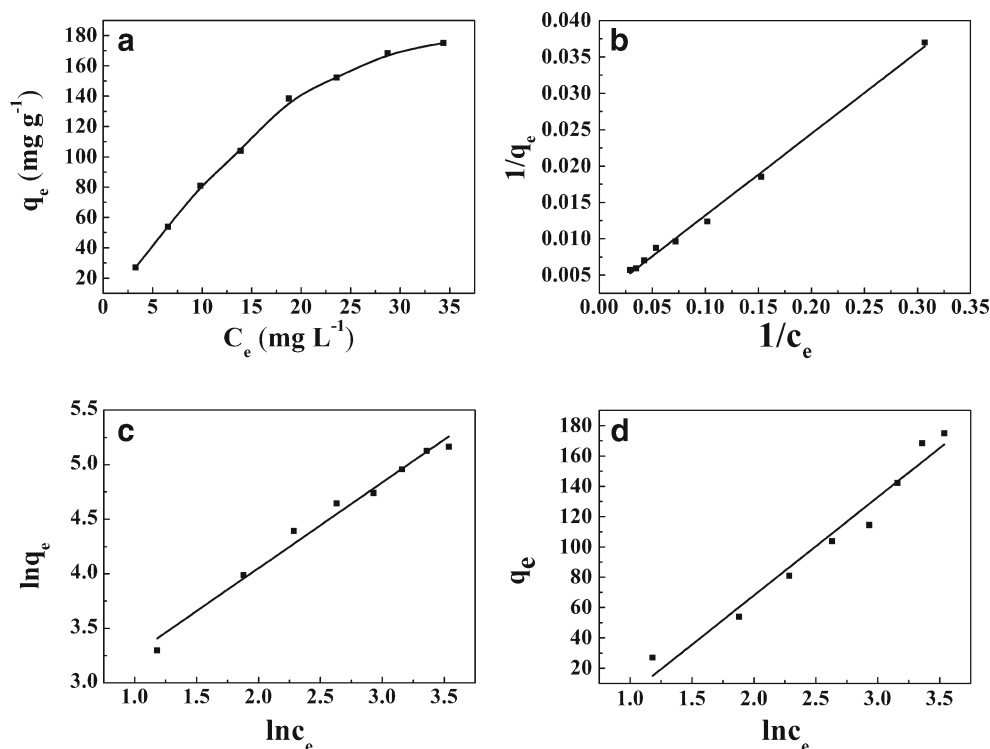
$$\frac{1}{q_e} = \frac{1}{bq_m C_e} + \frac{1}{q_m} \quad (2a)$$

$$\ln q_e = \frac{1}{n} \ln C_e + \ln K_f \quad (2b)$$

$$q_e = \frac{RT}{b_T} \ln C_e + \frac{RT}{b_T} \ln A_T \quad (2c)$$

where q_m (milligrams per gram) is the theoretical maximum adsorption capacity corresponding to complete monolayer

Fig. 10 Adsorption isotherms (a), linear Langmuir isotherm (b), linear Freundlich isotherm (c) and Temkin isotherm (d) of soluble diesel oil with graphene as the adsorbent at 25 °C



coverage; b , K_f , b_T are the adsorption constants of the Langmuir, Freundlich, and Temkin models, respectively; and n is the Freundlich linearity index.

The results of fitting these models were shown in Fig. 10b–d, and the fitting parameters for soluble diesel oil were listed in Table 4. In the range of tested concentration, the correlation coefficient of Langmuir model was very high ($R^2=0.9964$, $SD=4.682 \times 10^{-7}$), but the ideal maximum adsorption capacity (q_m) was determined by the Langmuir model to be 500 mg g^{-1} , which seriously deviated from the experimental equilibrium sorption capacity. These suggested that the Langmuir model was not fit to describe this adsorption process. Moreover, the Freundlich model ($R^2=0.9833$, $SD=0.00786$) fits the adsorption data well, in comparison with the Temkin model ($R^2=0.9672$, $SD=107.1$). So, the Freundlich model could fit best. The intercept K_f obtained from Freundlich model was a rough measurement of the sorption capacity and the slope ($1/n$) of the sorption intensity (Poots et al. 1978). Low value of $1/n$ indicated more heterogeneous adsorption process. Below unity values of $1/n$ indicated chemisorptions (Zeldowitsch 1934). Using the Freundlich model, the value of $1/n$ at equilibrium was less than 1 (Table 3), suggesting chemical adsorption (Zeldowitsch

1934), which agreed with the results of pseudo-second-order kinetic models.

The adsorption mechanism of soluble oil on graphene is not clear yet. In the present work, we put forth some assumptions regarding the adsorption process based on the above analysis. As the surface defects of the material increase, there would be an increased presence of high-energy adsorption sites, which could cause heterogeneous adsorption. Soluble oil could first occupy high-energy adsorption sites and then spread to sites with lower energy (Agnihotri et al. 2008). Moreover, the large surface area and the high surface hydrophobicity of graphene enabled a strong adsorption affinity and capacity for soluble oil. Furthermore, the graphene honeycomb lattice was composed of two equivalent sub-lattices of carbon atoms bonded together with σ bonds, and each carbon atom in the lattice had a π orbital that contributed to a delocalized network of electrons (Zhu et al. 2010). Additionally, soluble oil was mainly composed of low-molecular-weight PAHs; thus, soluble oil was adsorbed on graphene by π - π stacking interactions (Guo et al. 2011, Rochefort and Wuest 2009, Waters 2013). The adsorption driving force was dominated by π - π stacking interactions, which were the

Table 4 Isotherm parameters for the adsorption of diesel oil by graphene

Sample	Langmuir isotherm				Freundlich isotherm				Temkin isotherm			
	q_m (mg g^{-1})	b (L mg^{-1})	R^2	SD	n	K_f	R^2	SD	A_T (L mg^{-1})	b_T	R^2	SD
Diesel oil	500	0.01779	0.9964	4.682×10^{-7}	1.272	11.93	0.9833	0.00786	0.3861	38.22	0.9672	107.1

most widely recognized. Ji et al. reported that the strong adsorption of the aromatic compounds was mainly due to π - π electron donor-acceptor interactions with the hexagonal structure of graphene (Ji et al. 2013). Tetracycline could be adsorbed by graphene oxide due to the π - π stacking interaction between the ring structure in the tetracycline and the hexagonal cells of the graphene oxide (Gao et al. 2012). π - π interaction was also found to be the dominating force for adsorption of aromatic and anti-aromatic systems on graphene (Bjoerk et al. 2010). These results suggested that adsorption process combines physical adsorption with chemisorption.

Conclusions

We have successfully prepared graphene using oxidation and thermal reduction methods. SEM, TEM, XRD, and Raman spectra analysis indicated that the graphite oxide has exfoliated into a monolayer or graphene lattices with fewer layers. BET analysis showed that graphene possessed a large surface area and bimodal pore size distribution, which provided the soluble oil molecules with suitable access to the interior. Contact angle analysis demonstrated that graphene had better superhydrophobic-superoleophilic characteristics. Meanwhile, it was found that soluble diesel oil, with an initial concentration of 76.86 mg L^{-1} , had an equilibrium adsorption capacity of 241.88 mg g^{-1} , and soluble crude oil, with an initial concentration of 2.638 mg L^{-1} , had an equilibrium adsorption capacity of 9.980 mg g^{-1} . The adsorption rate of soluble oil on graphene was notably rapid, especially for soluble diesel oil, which could reach equilibrium within 30 min, and the kinetics of adsorption fit the pseudo-second-order model perfectly. The adsorption isotherm fit the Freundlich model well. Moreover, soluble oil molecules were strongly adsorbed on the surface of graphene by hydrophobic interactions, π - π bonds, and van der Waals interactions. This adsorption process combined physical adsorption with chemisorption. Furthermore, a deep and comprehensive understanding of the adsorption mechanism requires further research.

Acknowledgments The authors are grateful for the financial support of this research from Tianjin Program of Science and Technology for Ocean Promotion (Grant No. KJXH2011-10).

References

- Agnihotri S, Kim P, Zheng Y, Mota JPB, Yang L (2008) Regioselective competitive adsorption of water and organic vapor mixtures on pristine single-walled carbon nanotube bundles. *Langmuir* 24: 5746–5754
- Allen MJ, Tung VC, Kaner RB (2010) Honeycomb carbon: a review of graphene. *Chem Rev* 110:132–145
- Atlas RM (1981) Microbial degradation of petroleum hydrocarbons: an environmental perspective. *Microbiol Rev* 45:180–209
- Bjoerk J, Hanke F, Palma C, Samori P, Cecchini M, Persson M (2010) Adsorption of aromatic and anti-aromatic systems on graphene through π - π stacking. *J Phys Chem Lett* 1:3407–3412
- Chen W, Yan L, Bangal PR (2010) Preparation of graphene by the rapid and mild thermal reduction of graphene oxide induced by microwaves. *Carbon* 48:1146–1152
- Cong H, Ren X, Wang P, Yu S (2012) Macroscopic multifunctional graphene-based hydrogels and aerogels by a metal ion induced self-assembly process. *ACS NANO* 6:2693–2703
- Deo N, Ali M (1993) Dye adsorption by a new low cost material: Congo red-1. *Indian J Environ Prot* 13:496–508
- Dreyer DR, Park S, Bielawski CW, Ruoff RS (2010) The chemistry of graphene oxide. *Chem Soc Rev* 39:228–240
- Ferrari AC, Robertson J (2000) Interpretation of Raman spectra of disordered and amorphous carbon. *Phys Rev B* 61:14095–14107
- Ferrari AC, Meyer JC, Scardaci V, Casiraghi C, Lazzeri M, Mauri F, Piscanec S, Jiang D, Novoselov KS, Roth S, Geim AK (2006) Raman spectrum of graphene and graphene layers. *Phys Rev Lett* 97:187401
- Freundlich HMF (1906) Over the adsorption in solution. *J Phys Chem* 57: 385–470
- Gao Y, Li Y, Zhang L, Huang H, Hu J, Shah SM, Su X (2012) Adsorption and removal of tetracycline antibiotics from aqueous solution by graphene oxide. *J Colloid Interface Sci* 368:540–546
- Gonzalez JJ, Vinas L, Franco MA, Fumega J, Soriano JA, Grueiro G, Muniategui S, Lopez-Mahia P, Prada D, Bayona JM, Alzaga R, Albaiges J (2006) Spatial and temporal distribution of dissolved/dispersed aromatic hydrocarbons in seawater in the area affected by the Prestige oil spill. *Mar Pollut Bull* 53:250–259
- Guo Y, Deng L, Li J, Guo S, Wang E, Dong S (2011) Hemin-graphene hybrid nanosheets with intrinsic peroxidase-like activity for label-free colorimetric detection of single-nucleotide polymorphism. *ACS NANO* 5:1282–1290
- Han CC, Lee JT, Chang H (2001) Thermal annealing effects on structure and morphology of micrometer-sized carbon tubes. *Chem Mater* 13: 4180–4186
- Hannam ML, Bamber SD, John Moody A, Galloway TS, Jones MB (2010) Immunotoxicity and oxidative stress in the Arctic scallop *Chlamys islandica*: effects of acute oil exposure. *Ecotoxicol Environ Saf* 73:1440–1448
- Harper N, Steinberg M, Safe S (1996) Immunotoxicity of a reconstituted polynuclear aromatic hydrocarbon mixture in B6C3F1 mice. *Toxicology* 109:31–38
- Hayase G, Kanamori K, Fukuchi M, Kaji H, Nakanishi K (2013) Facile synthesis of marshmallow-like macroporous gels usable under harsh conditions for the separation of oil and water. *Angew Chem Int Ed* 52:1986–1989
- Ho YS, McKay G (1998) Sorption of dye from aqueous solution by peat. *Chem Eng J* 70:115–124
- Ho YS, Ng J, McKay G (2000) Kinetics of pollutant sorption by biosorbents: review. *Sep Purif Method* 29:189–232
- Hsieh CT, Chen WY (2010) Water/oil repellency and drop sliding behavior on carbon nanotubes/carbon paper composite surfaces. *Carbon* 48:612–619
- Hsieh CT, Chen WY (2011) Water/oil repellency and work of adhesion of liquid droplets on graphene oxide and graphene surfaces. *Surf Coat Technol* 205:4554–4561
- Iqbal MZ, Abdala AA (2012) Oil spill cleanup using graphene. *Environ Sci Pollut Res* 20:1–9
- Ji L, Chen W, Xu Z, Zheng S, Zhu D (2013) Graphene nanosheets and graphite oxide as promising adsorbents for removal of organic contaminants from aqueous solution. *J Environ Qual* 42:191–198
- Kannan N (1991) A study on removal of nickel by fly ash. *Indian J Environ Prot* 11:514

- Kannan N, Sundaram MM (2001) Kinetics and mechanism of removal of methylene blue by adsorption on various carbons—a comparative study. *Dye Pigment* 51:25–40
- Kennedy CJ, Farrell AP (2005) Ion homeostasis and interrenal stress responses in juvenile Pacific herring, *Clupea pallasii*, exposed to the water-soluble fraction of crude oil. *J Exp Mar Biol Ecol* 323:43–56
- Kim KS, Zhao Y, Jang H, Lee SY, Kim JM, Kim KS, Ahn J, Kim P, Choi J, Hong BH (2009) Large-scale pattern growth of graphene films for stretchable transparent electrodes. *Nature* 457:706–710
- Korhonen JT, Kettunen M, Ras RHA, Ikkala O (2011) Hydrophobic nanocellulose aerogels as floating, sustainable, reusable, and recyclable oil absorbents. *ACS Appl Mater Interfaces* 3:1813–1816
- Kudin KN, Ozbas B, Schniepp HC, Prud'Homme RK, Aksay IA, Car R (2008) Raman spectra of graphite oxide and functionalized graphene sheets. *Nano Lett* 8:36–41
- Langergren S, Svenska BK (1898) Zur theorie der sogenannten adsorption gelöster stoffe. *K Sven Vetenskapsakad Handl* 24:1–39
- Langmuir I (1916) The adsorption of gases on plane surface of glass, mica and platinum. *J Am Chem Soc* 40:1361–1368
- Le Dû-Lacoste M, Akcha F, Dévier M, Morin B, Burgeot T, Budzinski H (2013) Comparative study of different exposure routes on the biotransformation and genotoxicity of PAHs in the flatfish species, *Scophthalmus maximus*. *Environ Sci Pollut R* 20:690–707
- Leinweber FC, Lubda D, Cabrera K, Tallarek U (2002) Characterization of silica-based monoliths with bimodal pore size distribution. *Anal Chem* 74:2470–2477
- Lerf A, Buchsteiner A, Pieper J, Schottl S, Dekany I, Szabo T, Boehm HP (2006) Hydration behavior and dynamics of water molecules in graphite oxide. *J Phys Chem Solids* 67:1106–1110
- Li D, Zhu FZ, Li JY, Na P, Wang N (2012) Preparation and characterization of cellulose fibers from corn straw as natural oil sorbents. *Ind Eng Chem Res* 52:516–524
- Maatar W, Alila S, Boufi S (2013) Cellulose based organogel as an adsorbent for dissolved organic compounds. *Ind Crops Prod* 49:33–42
- McAllister MJ, Li J, Adamson DH, Schniepp HC, Abdala AA, Liu J, Herrera-Alonso M, Milius DL, Car R, Prud'Homme RK, Aksay IA (2007) Single sheet functionalized graphene by oxidation and thermal expansion of graphite. *Chem Mater* 19:4396–4404
- McKay G, Otterburn MS, Aja JA (1985) Fuller's earth and fired clay as adsorbents for dyestuffs. *Water Air Soil Pollut* 24:307–322
- Meador JP, Stein JE, Reichert WL, Varanasi U (1995) Bioaccumulation of polycyclic aromatic hydrocarbons by marine organisms. *Reviews of environmental contamination and toxicology*. Springer, New York, pp 79–165
- Meyer JC, Geim AK, Katsnelson MI, Novoselov KS, Booth TJ, Roth S (2007) The structure of suspended graphene sheets. *Nature* 446:60–63
- Mohan D, Singh KP (2004) Single and multicomponent adsorption of cadmium and zinc using activated carbon derived from bagasse—an agricultural waste. *Water Res* 36:2304–2318
- Neff JM, Anderson JW (1981) Response of marine animals to petroleum and specific petroleum hydrocarbons.
- Nicolas M, Guittard F, Geribaldi S (2006) Synthesis of stable super water- and oil-repellent polythiophene films. *Angew Chem Int Ed* 45:2251–2254
- Novoselov KS, Geim AK, Morozov SV, Jiang D, Zhang Y, Dubonos SV, Grigorieva IV, Firsov AA (2004) Electric field effect in atomically thin carbon films. *Science* 306:666–669
- Pan D, Wang S, Zhao B, Wu M, Zhang H, Wang Y, Jiao Z (2009) Li storage properties of disordered graphene nanosheets. *Chem Mater* 21:3136–3142
- Paredes JL, Villar-Rodil S, Solis-Fernandez P, Martínez-Alonso A, Tascon J (2009) Atomic force and scanning tunneling microscopy imaging of graphene nanosheets derived from graphite oxide. *Langmuir* 25:5957–5968
- Poots V, McKay G, Healy JJ (1978) Removal of basic dye from effluent using wood as an adsorbent. *Water Pollut Cont Fed* 50:926–935
- Radetic M, Ilic V, Radojevic D, Miladinovic R, Jovic D, Jovancic P (2008) Efficiency of recycled wool-based nonwoven material for the removal of oils from water. *Chemosphere* 70:525–530
- Ray MS (1996) Adsorption and adsorptive separations: a review and bibliographical update. *Adsorption* 2:157–178
- Rochefort A, Wuest JD (2009) Interaction of substituted aromatic compounds with graphene. *Langmuir* 25:210–215
- Sato K, Saito R, Oyama Y, Jiang J, Cancado LG, Pimenta MA, Jorio A, Samsonidze GG, Dresselhaus G, Dresselhaus MS (2006) D-band Raman intensity of graphitic materials as a function of laser energy and crystallite size. *Chem Phys Lett* 427:117–121
- Schniepp HC, Li JL, McAllister MJ, Sai H, Herrera-Alonso M, Adamson DH, Prud'Homme RK, Car R, Saville DA, Aksay IA (2006) Functionalized single graphene sheets derived from splitting graphite oxide. *J Phys Chem B* 110:8535–8539
- Stankovich S, Dikin DA, Dommett GHB, Kohlhaas KM, Zimney EJ, Stach EA, Piner RD, Nguyen ST, Ruoff RS (2006) Graphene-based composite materials. *Nature* 442:282–286
- Stankovich S, Dikin DA, Piner RD, Kohlhaas KA, Kleinhammes A, Jia Y, Wu Y, Nguyen ST, Ruoff RS (2007) Synthesis of graphene-based nanosheets via chemical reduction of exfoliated graphite oxide. *Carbon* 45:1558–1565
- Steurer P, Wissert R, Thomann R, Muelhaupt R (2009) Functionalized graphenes and thermoplastic nanocomposites based upon expanded graphite oxide. *Macromol Rapid Comm* 30:316–327
- Sun H, Xu Z, Gao C (2013) Multifunctional, ultra-flyweight, synergistically assembled carbon aerogels. *Adv Mater* 25:2554–2560
- Temkin MJ, Pyzhev V (1940) Recent modifications to Langmuir isotherms. *Acta Physicochim URSS* 12:217–222
- Toyoda M, Inagaki M (2003) Sorption and recovery of heavy oils by using exfoliated graphite. *Spill Sci Technol B* 8:467–474
- Ueta H, Saida M, Nakai C, Yamada Y, Sasaki M, Yamamoto S (2004) Highly oriented monolayer graphite formation on Pt(111) by a supersonic methane beam. *Surf Sci* 560:183–190
- Vimonses V, Lei S, Jin B, Chow CW, Saint C (2009) Kinetic study and equilibrium isotherm analysis of Congo Red adsorption by clay materials. *Chem Eng J* 148:354–364
- Voloshina EN, Mollenhauer D, Chiappisi L, Paulus B (2011) Theoretical study on the adsorption of pyridine derivatives on graphene. *Chem Phys Lett* 510:220–223
- Wang S, Zhang Y, Abidi N, Cabrales L (2009) Wettability and surface free energy of graphene films. *Langmuir* 25:11078–11081
- Wang J, Zheng Y, Wang A (2012) Effect of kapok fiber treated with various solvents on oil absorbency. *Ind Crop Prod* 40:178–184
- Waters ML (2013) Aromatic interactions. *Acc Chem Res* 46:873–873
- Weber WJ, Morris JC (1963) Kinetics of adsorption on carbon from solution. *J Sanit Eng Div Am Soc Civ Eng* 89:31–60
- Yang et al (2009) Chemical analysis of graphene oxide films after heat and chemical treatments by X-ray photoelectron and micro-Raman spectroscopy. *Carbon* 47:145–152
- Zeldowitsch J (1934) Adsorption site energy distribution. *Acta Physicochim URSS* 1:961–973
- Zhao X, Zhang Q, Chen D, Lu P (2010) Enhanced mechanical properties of graphene-based poly (vinyl alcohol) composites. *Macromolecules* 43:2357–2363
- Zhu Y, Murali S, Cai W, Li X, Suk JW, Potts JR, Ruoff RS (2010) Graphene and graphene oxide: synthesis, properties, and applications. *Adv Mater* 22:3906–3924
- Zioli RL, Jardim WF (2002a) Photocatalytic decomposition of seawater-soluble crude-oil fractions using high surface area colloid nanoparticles of TiO₂. *J Photochem Photobiol A* 147:205–212
- Zioli RL, Jardim WF (2002b) Operational problems related to the preparation of the seawater soluble fraction of crude oil. *J Environ Monit* 4:138–141